Energy flow around a small particle investigated by classical Mie theory

Z. B. Wang,[1,2] B. S. Luk'yanchuk,[1,3,*] M. H. Hong,[1,2] Y. Lin,[1,2] and T. C. Chong[1,2]

[1]*Data Storage Institute, DSI Building, 5 Engineering Drive 1, Singapore 117608, Republic of Singapore*

[2]*Department of Electrical and Computer Engineering, National University of Singapore, Singapore 117576, Republic of Singapore*

[3]*Research Centre of Wave Studies, General Physics Institute, Russian Academy of Sciences Vavilova 38, Moscow, Russia, 117492*

The field lines of Poynting vector around a small particle are investigated on the basis of classical Mie theory. A particle can effectively absorb incident energy near the optical resonance, where its optical absorption cross-section becomes much greater than its geometrical cross-section. It is shown that absorbed energy flows into the particle through some limited portion of its surface ("input window") instead of the whole surface as it follows from the dipole approximation. This "input window" expands with the increasing value of the imaginary part ε'' of the dielectric function of the particle. For a small ε'' the absorbed energy is released by the plasmon radiation. Interference of this radiation with the incident wave creates complex patterns of energy flux in the near-field region. These patterns cannot be understood within the frame of a dipole approximation and the terms of higher orders with respect to size parameter $q=2\pi a/\lambda$ (a is the radius of the particle and λ is radiation wavelength) should be taken into account.

I. INTRODUCTION

The problem of light scattering by spherical particles has an exact solution presented by the classical Mie theory.[1–3] The fields around small particles are generally investigated in terms of specific far-field quantities such as absorption, scattering and extinction cross-sections or its far-field scattering diagram. These far-field characteristics are sufficient to explain the color of glasses (with embedded metallic nanoclusters) and the absorption of colloids, characteristics of the cosmic interstellar dust (Milky Way) and many other effects in meteorology and optical tomography. More detailed information follows from the analysis of near-field effects and the investigation of the energy flux (Poynting vector). Although this problem also refers to the classical problem of electromagnetism, it continues to attract attention until now; see, e.g., Refs. 4–7. Due to the development of nanotechnologies this problem became especially important lately due to the study of light scattering by *small particles*. It is important for many modern applications, e.g., for field concentration for nanopatterning,[8–10] near-field optical microscopy and other studies,[11–13] laser cleaning,[14,15] high-Q cavity devices,[16–19] nonlinear optics in microspheres,[20] surface enhanced Raman scattering,[21,22] plasmon resonance coupling in nanowires,[23] or within the chain of coupling nanoparticles.[11,18]

In spite of the importance of the mentioned problems, little attention has been paid to the investigation of the energy flux around small particles. To the best of our knowledge, Bohren published the first work in this field in 1983 within the frame of dipole approximations.[24] He demonstrated that the energy flux in the vicinity of a small particle deflects towards the particle from the surrounding area. The graphic illustration in Ref. 24 presents the near-field problem in a new impressive manner (field lines enter into the particle not only from the front but also from the back "shadow" side). As a result the particle can absorb much more radiation than that given by the geometrical cross-section. This presentation clearly explains the growth of the particle absorption process for small ε'' near plasmon resonance frequency, $\omega=\omega_p$, when $\varepsilon(\omega_p)=-2+i\varepsilon''$. It should be mentioned, according to Ref. 24, that the absorption cross-section increases inversely proportional to ε''.

In spite of the successes with an explanation of the absorption problem in Ref. 24, some questions still remain unclear. For example, it is very questionable that the particle absorbs incident energy through its whole surface, as shown in Ref. 24. This question stems from the fact that the refractive index of the particle $n=\mathrm{Re}\sqrt{\varepsilon'+i\varepsilon''}$ with $\varepsilon'=-2$ becomes smaller than 1 when $\varepsilon''<3.464$. From the geometrical optics point of view (when a particle is big compared to λ), some incident rays cannot "enter" the particle due to total internal reflection. In other words, a particle with a small ε'' value should absorb incident energy just through some "*input window*" on its surface and this window should be smaller and smaller with decreasing ε''.

Another contradiction follows from certain peculiarities of the resonant scattering by a very small particle. As it was shown by Tribelsky,[25] when the imaginary part of the permittivity is small enough, a nondissipative damping of the incident electromagnetic wave replaces the dissipative damping in the stabilization of divergence of the small particle extinction (absorption) cross-section at the resonance point. While the increase of the cross-section at the resonance is related to transformation of the incident electromagnetic wave into plasmons, the nondissipative damping is associated with the inverse transformation of the plasmons into the scattered electromagnetic wave. Due to the nondissipative damping the extinction cross-section remains finite up to the limit $\varepsilon''=0$. Although the field fluxes were not investigated in Ref. 25, one can expect that this emission–reabsorption process should produce the energy flux that *leaves and enters* the particle.

　　　　　　70 035418-1

Finally, metallic nanoparticles were successfully used for nanopatterning.[26,27] It indicates that these kinds of particles should produce the *outward* flux of energy in the near-field region, i.e., along with the "*input window*" there should be another "*output window*" for the energy flux.

To solve the contradiction with the incoming flux, which can enter the particle from any direction, we have analyzed this energy flux more precisely, taking into account the next small term within the Mie series expansion. One should remember that the dipole approximation for the field has been used in Ref. 24. The phase portrait of the energy flow that comes from this approximation contains a *single saddle point* outside the particle (here we do not concern a singular point inside the particle). It is shown that the "small perturbation" which follows from the next term in the Mie series, however, can change drastically this phase portrait where *five additional singular points* arise (outside the particle). However this phase portrait is still not stable, i.e., the inclusion of further terms in the Mie series changes this portrait qualitatively. With some sufficient number of terms a stable picture is established. The number of these terms depends on q and ε values. Even when this number is small (e.g., 3–4 terms) one should work beyond the dipole approximation to explain the peculiarities of the phase portrait in the near-field region. The stable energy flux for a small value of ε'' demonstrates "*input*" and "*output*" energy windows on the particle surface, as well as fluxes emitted and reabsorbed by the particle. The last radiation field (similar to the evanescent wave) is confined in a small region near the particle. With a sufficiently big value of ε'' stable flux is similar to those found by Bohren with a dipole approximation in Ref. 24. In the intermediate region of parameter ε'' other stable phase portraits with different singularities within the Poynting vector field are possible. The complex field patterns in the near-field region of a small particle can be used for the enhancement of both electric and magnetic fields.

II. ENERGY FLUX AND THE FIELD LINES OF THE POYNTING VECTOR

Geometrical optics[28] yields the simplest approach to understand the energy flux within the weakly absorbing media. This approach is applicable for particles (radius a) with a size significantly larger than the radiation wavelength, e.g., $a \gg \lambda$. In this case the intensity distribution around the particle can be estimated using ray tracing according to Snell's law and energy conservation. For a particle with refractive index $1 < n < 2$ in vacuum, the refracted rays form a caustic[15] under the particle. At plasmon resonance with $\varepsilon = -2 + i\varepsilon''$, one can see that within a big range of $\varepsilon'' < 3.464$, the refractive index of the particle $n = \mathrm{Re}\sqrt{\varepsilon}$ is smaller than one. For such a case the vacuum ($n=1$) is an optically denser media than the particle, which results in the total internal reflection and some incident rays are thus forbidden to "enter" the particle, as shown in Fig. 1. For a small value of n the "*input window*" on the particle surface becomes very small. This picture illustrates an interesting effect: a particle can transfer energy from the near-field region to a far-field region just through a very small "effective aperture," $y/a \approx \arctan n$,
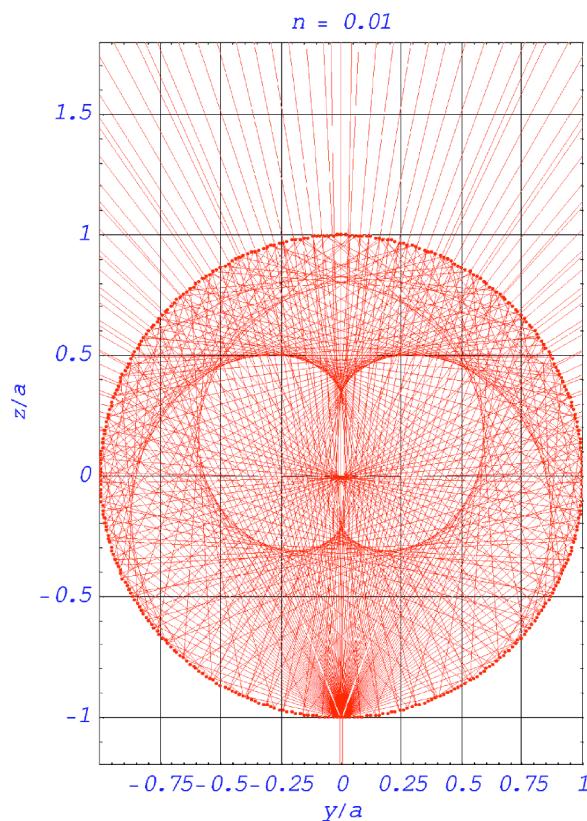

FIG. 1. (Color online) Rays tracing for a big particle with $a \gg \lambda$ and refractive index $n = 0.01$. The incidence angle θ_i outside of the sphere and the refraction angle θ_t inside the sphere are related by $\theta_t = \arcsin[\sin \theta_i / n]$. The rays with input coordinate $y/a > \arctan(n)$ cannot enter into the particle due to the total internal reflection effect. Within the figure the caustics inside the particle are shown for two subsequent reflections.

created by total internal reflection. The energy conversion by this aperture can be significantly higher than that within the scanning near-field optical microscope (SNOM) system, where this conversion efficiency is $10^{-4} - 10^{-5}$.[29] At the same time the validity of geometrical optics is frustrated: with a small aperture the diffraction effect should play an important role. It is clear that absorption also frustrates total internal reflection and the true scattering problem should be analyzed on the basis of the Mie theory.

Examples of these calculations for the electric and magnetic fields are shown in Fig. 2. Plasmon are localized near the surface.[30] The fields distributions are typical for dipole radiation. One can see that the electric field mainly concentrates along "left" and "right" surfaces, while the magnetic field is localized near the "top" and "bottom" surfaces. This picture however does not tell much about the peculiarities of energy flux propagation. For this purpose we should calculate the energy flux, i.e., the Poynting vector.

The Mie solution is based upon the expansion of the incident wave, the scattered wave and the wave interior of the particle into corresponding vector spherical harmonics. Similar to Ref. 24 we consider a vacuum media and a nonmagnetic particle, i.e., $\varepsilon_m = \mu_m = \mu_p = 1$ (ε_m and ε_p stand for the permittivities of the media and the particle, μ_m and μ_p are
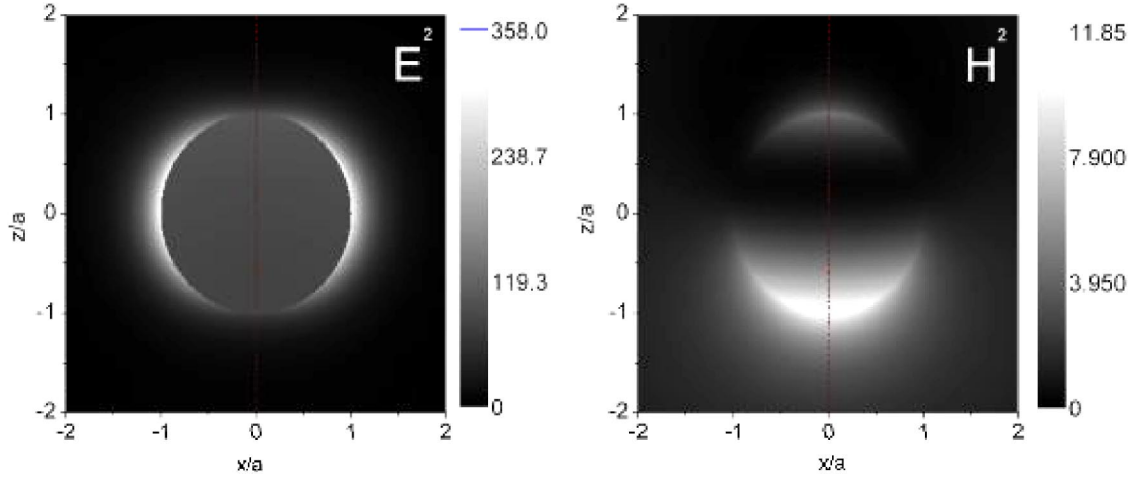
FIG. 2. Electric $\mathbf{E}^2 = \mathbf{E} \cdot \mathbf{E}^*$ and magnetic $\mathbf{H}^2 = \mathbf{H} \cdot \mathbf{H}^*$ fields distributions within the xz-plane, calculated from the Mie theory for a sphere with a size parameter $q = 2\pi a / \lambda = 0.3$ and dielectric function $\varepsilon = -2 + 0.2\,i$. Incident electric field $\mathbf{E}^{(i)}$ is directed along the x-axis.

their magnetic permeabilities) and the incident electric field that is polarized along the x-axis and propagates along the positive z direction. The incident plane wave has components $E_i = E_0 e^{ikz} \hat{e}_x$ and $H_i = E_0 e^{ikz} \hat{e}_y$, where wave vector $k = 2\pi c / \lambda$. Time dependence $e^{-i\omega t}$ is omitted and we also consider the unit amplitude $E_0 = 1$. These incident fields in spherical coordinates are given by

$$E_r = e^{ikr \cos\theta} \sin\theta \cos\varphi, \quad E_\theta = e^{ikr \cos\theta} \cos\theta \cos\varphi,$$

$$E_\varphi = -e^{ikr \cos\theta} \sin\varphi,$$

$$H_r = e^{ikr \cos\theta} \sin\theta \sin\varphi, \quad H_\theta = e^{ikr \cos\theta} \cos\theta \sin\varphi,$$

$$H_\varphi = e^{ikr \cos\theta} \cos\varphi. \tag{1}$$

For fields scattered by a sphere with radius a, the fields can be expressed through electric ${}^e\Pi^{(s)}$ and magnetic ${}^m\Pi^{(s)}$ Debye potentials:

$$r\,{}^e\Pi^{(s)} = -\frac{\cos\varphi}{k^2} \sum_{\ell=1}^{\infty} {}^eB_\ell\, \zeta_\ell(kr)\, P_\ell^{(1)}(\cos\theta),$$

$$r\,{}^m\Pi^{(s)} = -\frac{\sin\varphi}{k^2} \sum_{\ell=1}^{\infty} {}^mB_\ell\, \zeta_\ell(kr)\, P_\ell^{(1)}(\cos\theta), \tag{2}$$

where $P_\ell^{(1)}(\cos\theta)$ is an associated Legendre polynomial and $\zeta_\ell(\rho) = \sqrt{\pi\rho/2}\, H_{\ell+1/2}^{(1)}(\rho)$, is a Ricatti-Bessel function, $H_n^{(1)}(\rho) = J_n(\rho) + i\, N_n(\rho)$ is the Hankel function. Coefficients ${}^eB_l$ and ${}^mB_l$ are presented by

$${}^eB_\ell = i^{\ell-1} \frac{2\ell+1}{\ell(\ell+1)} a_\ell,$$

$${}^mB_\ell = i^{\ell-1} \frac{2\ell+1}{\ell(\ell+1)} b_\ell,$$

$$a_\ell = \frac{q_p\, \psi_\ell(q_p)\, \psi_\ell'(q) - q\, \psi_\ell(q)\, \psi_\ell'(q_p)}{q\, \zeta_\ell(q)\, \psi_\ell'(q_p) - q_p\, \zeta_\ell'(q)\, \psi_\ell(q_p)},$$

$$b_\ell = \frac{q\, \psi_\ell(q_p)\, \psi_\ell'(q) - q_p\, \psi_\ell(q)\, \psi_\ell'(q_p)}{q_p\, \zeta_\ell(q)\, \psi_\ell'(q_p) - q\, \zeta_\ell'(q)\, \psi_\ell(q_p)}, \tag{3}$$

where $q = ka$ is the size parameter and $q_p = q\sqrt{\varepsilon_p}$. $\psi_\ell(\rho) = \sqrt{\pi\rho/2}\, J_{\ell+1/2}(\rho)$, where $J_n(\rho)$ is the Bessel function. For a small particle with $q \ll 1$ one can see from the expansion of the Bessel and Hankel functions that the electric amplitude ${}^eB_\ell \sim q^{2\ell+1}$ is much greater than the magnetic amplitude ${}^mB_\ell \sim q^{2\ell+3}$ (the $q^{2\ell+1}$ term in ${}^mB_\ell$ expansions is zero since it is proportional to $\mu_p - \mu_m$). Expanding separately the numerator and denominator in ${}^eB_\ell$ with accuracy to $q^{2\ell+1}$ terms one can find the formula

$${}^eB_\ell = i^\ell\, q^{2\ell+1} \frac{\varepsilon_p - 1}{[(2\ell-1)!!]^2} \left\{ \ell^2 \left(\varepsilon_p + \frac{\ell+1}{\ell} \right) \right.$$

$$\left. - i\, q^{2\ell+1} \frac{\varepsilon_p - 1}{[(2\ell-1)!!]^2} \frac{\ell(\ell+1)}{2\ell+1} \right\}^{-1}. \tag{4}$$

It is clear from Eq. (4) that for the exact ℓ-th order resonance, when $\varepsilon_p = -(\ell+1)/\ell$ the amplitude tends to its limiting value ${}^eB_\ell = i^{\ell+1}(2\ell+1)/\ell(\ell+1)$. This case corresponds to "nondissipative damping," as discussed in Ref. 25. In the following, we will first discuss the first order plasmon resonance with $\ell = 1$, where $\mathrm{Re}(\varepsilon_p) = -2$. For $\mathrm{Im}(\varepsilon_p) \gg 2q^3$ one can use the approximation

$${}^eB_1 = i \frac{\varepsilon_p - 1}{\varepsilon_p + 2} q^3. \tag{5}$$

The electric and magnetic fields scattered by a sphere can be expressed by differentiation of Debye potentials:[1]

$$E_r^{(s)} = \left(\frac{\partial^2}{\partial r^2} + k^2 \right)(r\,{}^e\Pi), \quad H_r^{(s)} = \left(\frac{\partial^2}{\partial r^2} + k^2 \right)(r\,{}^m\Pi),$$

$$E_\theta^{(s)} = \frac{1}{r} \frac{\partial^2}{\partial\theta\,\partial r}(r\,{}^e\Pi) + \frac{ik}{r\sin\theta} \frac{\partial}{\partial\varphi}(r\,{}^m\Pi),$$

$$H_\theta^{(s)} = -\frac{i\,k}{r\,\sin\,\theta}\frac{\partial}{\partial\,\varphi}(r\ ^e\Pi) + \frac{1}{r}\frac{\partial^2}{\partial\,\theta\,\partial\,r}(r\ ^m\Pi),$$

$$E_\varphi^{(s)} = \frac{1}{r\,\sin\,\theta}\frac{\partial^2}{\partial\,\varphi\,\partial\,r}(r\ ^e\Pi) - \frac{ik}{r}\frac{\partial}{\partial\,\theta}(r\ ^m\Pi),$$

$$H_\varphi^{(s)} = \frac{ik}{r}\frac{\partial}{\partial\,\theta}(r\ ^e\Pi) + \frac{1}{r\,\sin\,\theta}\frac{\partial^2}{\partial\,\varphi\,\partial\,r}(r\ ^m\Pi). \qquad (6)$$

For a small particle the lowest order terms for the field expansion are proportional to q^3:

$$E_r^{(s)} = 2\frac{\varepsilon_p - 1}{\varepsilon_p + 2}q^3\ e^{ikr}\frac{1 - ikr}{(kr)^3}\sin\,\theta\,\cos\,\varphi, \quad H_r^{(s)} = 0,$$

$$E_\theta^{(s)} = \frac{\varepsilon_p - 1}{\varepsilon_p + 2}q^3\ e^{ikr}\frac{-1 + ikr + (kr)^2}{(kr)^3}\cos\,\theta\,\cos\,\varphi,$$

$$H_\theta^{(s)} = \frac{\varepsilon_p - 1}{\varepsilon_p + 2}q^3\ e^{ikr}\frac{i + k\,r}{(kr)^2}\sin\,\varphi,$$

$$E_\varphi^{(s)} = -\frac{\varepsilon_p - 1}{\varepsilon_p + 2}q^3\ e^{ikr}\frac{-1 + ikr + (kr)^2}{(kr)^3}\sin\,\varphi,$$

$$H_\varphi^{(s)} = \frac{\varepsilon_p - 1}{\varepsilon_p + 2}q^3\ e^{ikr}\frac{i + k\,r}{(kr)^2}\cos\,\theta\,\cos\,\varphi. \qquad (7)$$

Within the far-field region, where $kr \gg 1$, Eqs. (7) produce the usual fields for a dipole approximation [see, e.g., Eqs. (88) in Chap. 14 of Ref. 1]. However we are interested in the near-field region where kr can be of the same order of magnitude as the size parameter q.

The Poynting vector $\mathbf{S} = (c/4\pi)\mathbf{E}\times\mathbf{H}$ specifies the magnitude and direction of the rate of transfer of electromagnetic energy at all points of space.[31,32] The total time-averaged Poynting vector can be written as

$$\langle\mathbf{S}\rangle = \langle S_i\rangle + \langle S_s\rangle + \langle S_{\text{ext}}\rangle, \qquad (8)$$

where

$$\langle S_i\rangle = \frac{c}{8\pi}\text{Re}\,(\mathbf{E_i}\times\mathbf{H_i^*}), \quad \langle S_s\rangle = \frac{c}{8\pi}\text{Re}(\mathbf{E_s}\times\mathbf{H_s^*}),$$

$$\langle S_{\text{ext}}\rangle = \frac{c}{8\pi}\text{Re}(\mathbf{E_i}\times\mathbf{H_s^*} + \mathbf{E_s}\times\mathbf{H_i^*}).$$

Here $\langle S_i\rangle$ is the Poynting vector of the incident field and $\langle S_s\rangle$ that of the scattered field. $\langle S_{\text{ext}}\rangle$ can be interpreted as the term which arises because of the interaction between the incident and scattered fields. In the zx plane ($\varphi = 0$), the φ component of vector $\langle S_i\rangle$ is zero and the field lines are described by the solutions to the differential equation

$$\frac{dr}{d\theta} = r\frac{\langle S\rangle_r}{\langle S\rangle_\theta}. \qquad (9)$$

Bohren[24] considers that the Poynting vector related to the scattered field does not affect Eq. (9) because of $\langle S\rangle_s \propto q^6$.

The substitution of Eq. (7) into (8) and (9) yields the differential equation:

$$\frac{d\rho}{d\theta} = -\rho\,\cot\,\theta\frac{F^{(\text{num})}}{F^{(\text{den})}}. \qquad (10)$$

Here $\rho = r/a$, functions $F^{(\text{num})} = \Sigma_{k=0}^3 g_k\rho^k$ and $F^{(\text{den})} = \Sigma_{k=0}^3 h_k\rho^k$ present polynomials with the highest term, which grows as ρ^3 at infinity, $\rho\rightarrow\infty$. Coefficients g_k and h_k are given by

$$g_0 = -(K_r\cos\,\xi + K_i\,\sin\,\xi),$$

$$g_1 = q(\cos\,\theta + 1)(K_r\sin\,\xi - K_i\cos\,\xi),$$

$$g_2 = q^2(\cos\,\theta + 1)(K_r\cos\,\xi + K_i\,\sin\,\xi), \quad g_3 = 1, \quad (11)$$

and

$$h_0 = 2\,(K_r\cos\,\xi + K_i\,\sin\,\xi),$$

$$h_1 = q\,(\cos\,\theta - 2)\,(K_r\sin\,\xi - K_i\cos\,\xi),$$

$$h_2 = q^2\cos\,\theta\,(K_r\cos\,\xi + K_i\,\sin\,\xi), \quad h_3 = 1. \qquad (12)$$

[The scattered field $\langle S\rangle_s$ yields additional term $q^4\cos\,\theta(K_r^2 + K_i^2)$ in g_1. This term has no important influence on the phase portrait.]

Following Ref. 24 we use notation $(\varepsilon_p - 1)/(\varepsilon_p + 2) \equiv K_r + iK_i$, and $\xi = q\rho(\cos\,\theta - 1)$. In regions far from the particle, where $\rho \gg 1$, Eq. (10) yields parallel Poynting vector lines with conserved coordinate $x = \rho\,\sin\,\theta = \text{const}$. The picture with the field lines according to Eq. (9) is presented in Fig. 3. This picture presents the phase portrait of the field lines with one singular point of the saddle type. (Another singular point is situated inside the particle. This point is, in fact, fictive because Poynting vector inside the particle is given by a different differential equation. Nevertheless one should remember about this point just to escape confusion with a variation of the Poincare index.) This saddle point (hereinafter referred to as the Bohren saddle point) is situated behind the particle at $x = 0$ and $z = 2.97$. The separatrix that goes thought this point separates different types of field lines. All the field lines under the separatrix enter the particle. A similar situation is typical for the field lines of a point charge moving in a constant electric field (see Fig. 1–Fig. 3 in Ref. 4).

The field lines which enter the particle correspond to the radial component of the Poynting vector at $r = a$. Under the Bohren approximation the value of the field enhancement is given by

$$\frac{\langle S_r(\theta)\rangle}{\langle S_i\rangle_z} = -\cos\,\theta\,(-1 + u_c\cos\,\xi - u_s\sin\,\xi),$$

$$u_c = (1 - q^2)K_r + qK_i + q(K_i - qK_r)\cos\,\theta,$$

$$u_s = qK_r - (1 - q^2)K_i + q(K_r + qK_i)\cos\,\theta. \qquad (13)$$

On the right part of Fig. 3 we presented these radial field lines (lengths are proportional to S_r) that enter the particle
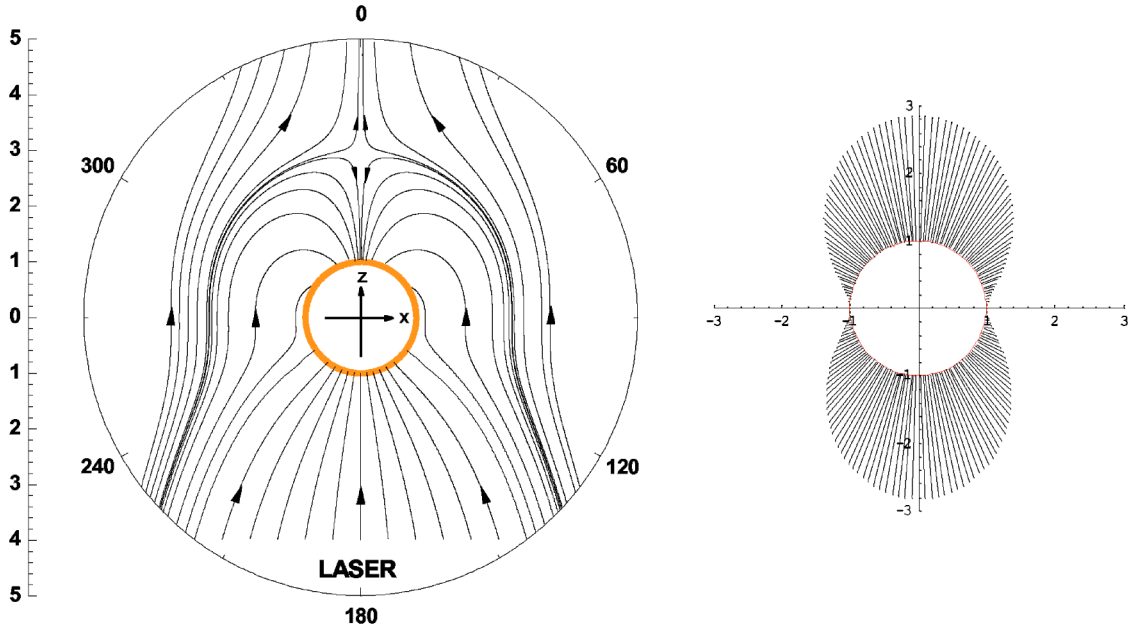
FIG. 3. Field lines of the Poynting vector found from Eq. (10) in the regions around a small particle with a size parameter $q=0.3$ and permittivity $\varepsilon_p=-2+0.2\,i$. On the right part of the figure the arrows present the radial component of the Poynting vector which enters the particle according to Eq. (13). Lengths of the arrows are proportional to the S_r value.

from all directions, from the front and from the backside ("shadow" region).

III. FIELD LINES OF THE POYNTING VECTOR BEYOND THE DIPOLE APPROXIMATION

It is clear that with an increasing value of the size parameter q one should take more than one term within the Mie series to reach a desirable accuracy. The recommended number of terms as given in Ref. 2 is $l_{max}=q+4.3\,q^{1/3}+1$. It means that the "true" Poynting field pattern should be calculated with sufficient order of scattered partial waves, e.g., for $q=0.3$ one should take four terms. In Fig. 4 we present the distribution of the Poynting vector component S_Z within the xy plane at $z/a=1$ (at the top of particle) and $z/a=-1$ (behind the particle at the "shadow" region). Calculations are performed with $q=0.3$ and other parameters are the same as in Fig. 3. All the necessary terms within the Mie series are taken into account. Figure 4 demonstrates an evident contradiction with the flux shown in Fig. 3. Namely, in the regions near the center $x=y=0$ the energy flux enters the particle through the "*input window*" [Fig. 4(a)] and leaves the particle through the "*output window*" [Fig. 4(b)]. The discrepancy between Figs. 3 and 4 looks like a paradox, which demonstrates that the dipole approximation is not applicable for a small particle.

To examine the influence of higher order partial waves, we take the second term within the Mie series and analyze the effect of the next small term in the field expansion. For this purpose one should consider the fields with terms proportional to q^5. These contributions arise from the first and second terms within the Mie series and one may write $E^{(s)}=E^1(q^3)+E^1(q^5)+E^2(q^5)$. Terms $E^1(q^3)$ are given by Eq. (7)

and terms $E^{1,2}(q^5)$ [and similar terms in magnetic field $H^{1,2}(q^5)$] are given in the Appendix.

Comparing E_θ components in Eq. (7) and Eq. (A1) for small q and ε'' (with $\varepsilon_p=-2+i\varepsilon''$) one can find $|E_\theta^1(q^5)/E_\theta^1(q^3)|\approx 2.4\,q^2/\varepsilon''$. It means that small q^2 value can be compensated by an even smaller ε'' value. For $q=0.3$ both terms yield the same contribution at $\varepsilon''=0.22$. It means that during the approach from dissipative damping to nondissipative damping the dipole approximation (with q^3 terms only) is insufficient. Thus we look for the next term in the expansion.
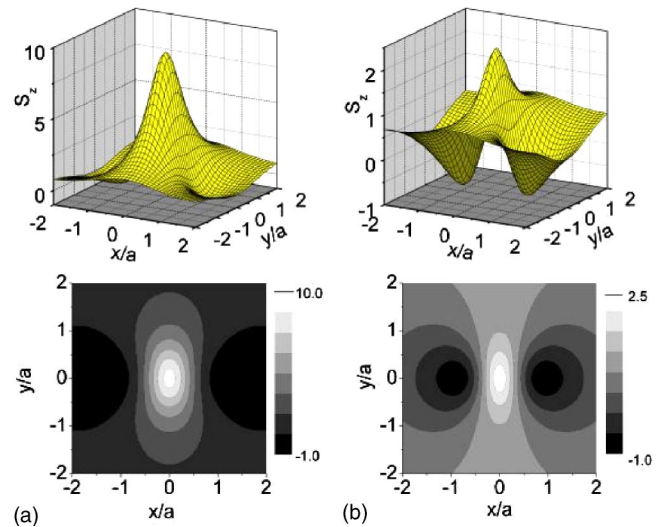

FIG. 4. (Color online) Distribution of the z-component of the Poynting vector within the xy-plane at (a) $z/a=-1$ (plane for incoming radiation) and (b) $z/a=1$ (plane for outgoing radiation).
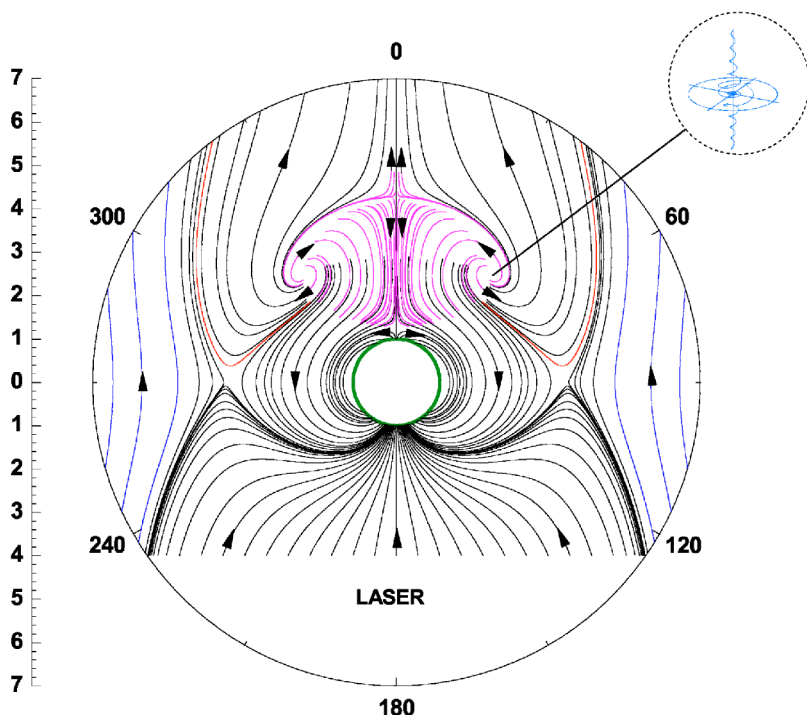
FIG. 5. (Color online) The same as in Fig. 3, but with the inclusion of q^5 terms for the scattered wave. Inset demonstrates 3-D phase trajectories near the saddle-focus point.

The laborious task to derive the differential equation (9) with scattered fields (7), (A1), and (A2) was done with the help of "MATHEMATICA" software.[33] Within the xz-plane (i.e., $\varphi=0$) this equation is presented in the form of Eq. (10), where the numerator $F^{(num)}=\Sigma_{k=0}^{4}u_k\rho^k$ and denominator $F^{(den)}=\Sigma_{k=0}^{4}w_k\rho^k$ are given by the fourth order of polynomials (with respect to ρ). This equation is also presented in the Appendix.

The field pattern according to this equation is shown in Fig. 5. One can see that a "small perturbation" related to higher order terms of a q value destroys the phase portrait in Fig. 3. The old Bohren's saddle point is stable, but moves up on the phase plane to $x=0$ and $z=4.28$. Nevertheless the behavior of separatrices that crossed this saddle point is now completely different. Moreover five additional singular points arise on the phase portrait in Fig. 5: three saddles and two foci [we changed the Poincare index by 2 during bifuracation (because of the singular point inside the particle)]. Two new saddle points (at $z=0$ and $x=\pm3.92$) control the flux, which enters the particle. Only field lines under separatrices from these saddle points enter the particle. As a result the energy enters the particle through a limited portion of surface ("*input window*") instead of the whole surface as shown in Fig. 3. The third saddle point behind the particle (situated close to the surface at $x=0$ and $z=1.25$) introduces the separatrix that separates field lines emitted and reabsorbed by the particle. This energy flux corresponds to the field that is emitted by plasmon in the case of a nondissipative damping effect. It is interesting that this field is localized in a small region that is comparable with the particle size.

Two foci ("energy vortices") are situated symmetrically ($x=\pm2.25$) at a distance $z=2.48$ behind the particle. They present the energy sources for the field lines in surrounding regions. Some of these field lines go to the particle and others go to the shadow region behind the particle (at $z>4$). The distribution of these fluxes is controlled by separatrices from the Bohren saddle point. In the three-dimensional (3-D) case it can be seen that these points are the saddle-focuses, i.e., the energy comes from perpendicular directions as it is shown in Fig. 4 (inset). In fact, similar optical vortices are known for the case of the speckle field produced by the interference of a plane wave with a Gaussian beam.[34]

The natural question arises: is this phase portrait stable or will it change further when the higher-order partial waves are taken into account. An analytical equation for this case becomes too complicated but we can easily analyze this problem numerically. After a series of calculations for $q=0.3$ and $\varepsilon''=0.2$ we found that phase portrait in Fig. 5 is also unstable. It becomes stable (i.e., it does not change further qualitatively) when the number of terms within the Mie series is equal to four. This stable pattern is presented in Fig. 6(a). One can see that this picture is quite simple; it contains the input and output windows for energy flux and waves, which present fluxes emitted by plasmon. In fact we expect a similar picture from the general physical consideration. It is interesting to note that down-directed fluxes of plasmon emission are concentrated in the surrounding of the xz-plane. In the yz-plane [see in Fig. 6(b)] all energy fluxes are directed up.

According to catastrophe theory,[35,36] the number of terms which one should take into account within the polynomials in the right hand part of Eq. (10) should satisfy the principal of "structural stability," i.e., the phase portrait should not change qualitatively with the addition of small perturbations arising from the higher-order terms of the Mie series. Naturally, a sufficient number of terms depends on the q and ε_p values.

Performing calculations based on an exact Mie solution and with an accuracy of expansion higher than q^6 one should take into account the field flux S_s in Eq. (8), related to the scattered wave. We found that with $0<\varepsilon''<1$ the number of

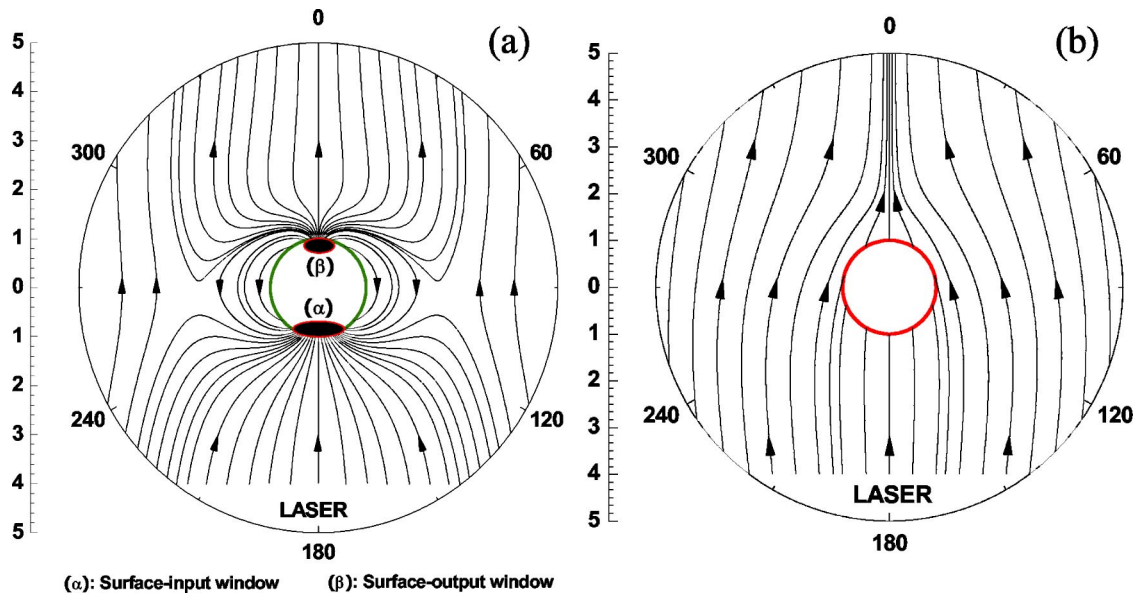(α): Surface-input window   (β): Surface-output window

FIG. 6. (Color online) (a) The field lines of the Poynting vector in the xz-plane calculated from the Mie theory for a particle with a size parameter $q=0.3$ and permittivity $\varepsilon_p=-2+0.2\,i$. The number of terms for the calculation was taken according to $\ell_{\max}=q+4.3\,q^{1/3}+1$. The surface-input window and surface-output window can be seen. (b) Field lines for the same parameters but in the yz-plane.

terms given by $\ell_{\max}=q+4.3\,q^{1/3}+1$ satisfies the condition of phase portrait stability. In Fig. 7 one can see variations of the input window for the energy flux. As ε'' decreases, the absorption cross-section of the particle increases while the input window shrinks. On the contrast, the output window is almost fixed for small values of ε''.

A few stable field patterns were identified for $q=0.3$ and ε'' within the range $0<\varepsilon''<1$. Patterns in Fig. 8 illustrate the energy fluxes when $\varepsilon''=0$. These patterns are of the same

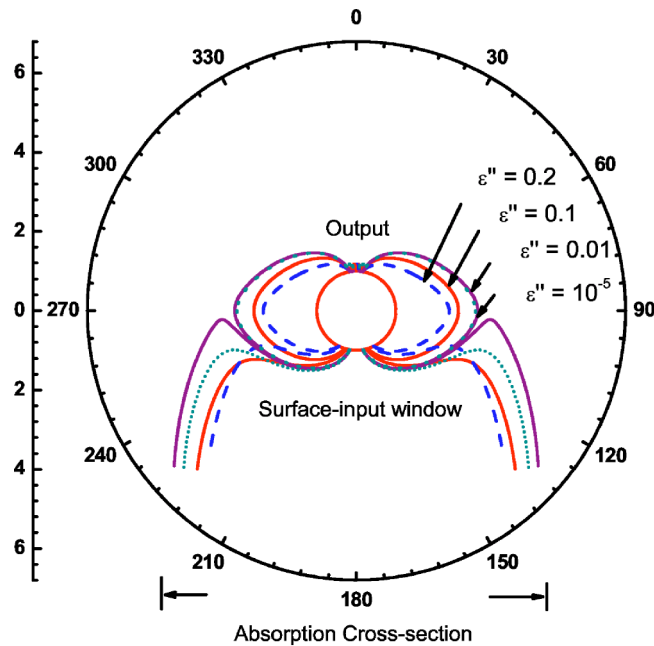
FIG. 7. (Color online) Variations in the surface-input window and surface-output window (in the xz-plane) for a particle with a size parameter $q=0.3$ and $\varepsilon_p=-2+i\varepsilon''$ where ε'' ranges from 10^{-5} to 0.2.

type as Fig. 6 with symmetry between the input and output fields. In exact plasmon resonance $\varepsilon=-2$ (Fig. 8 a) the scattering cross-section reaches its maximal value, which is not infinite. Out of resonance (Fig. 8 b) the picture is similar, but with a smaller cross-section. Negative (down-directed) flux emitted by plasmon is confined by a "banana"- shaped three-dimensional surface. We call these fluxes "*Tribelsky ears*" because they correspond to the nondissipative damping effect.[25] The cross-section of this energy flux structure by the xy-plane (through the particle center at $z=0$) is shown in Fig. 9.

To analyze transforms on phase portraits we use the standard methods of the theory of nonlinear oscillations.[37] First we search for the singular (stationary) points r_s, θ_s, which are the roots of equations for zero-isoclines: $\langle S(r,\theta)\rangle_r=0$ and $\langle S(r,\theta)\rangle_\theta=0$. These roots depend on parameters q and ε''. Solution $r_s=r_s(\varepsilon'')$ for $q=0.3$ is presented in the central port of Fig. 10. On the right picture the trajectories of the singular points on the xz-plane with a variation of ε'' parameter are shown. One can see along the ε'' parameter the regions with a different number of singular points.

(I) The first region $0<\varepsilon''<0.2892$ corresponds to a singular root $\rho=r_s/a$. This value varies from 3.4 to 2.1 within the discussed region (and continues to the particle surface $\rho=1$ with higher values of ε''). This root however is degenerated; it corresponds to two different values of θ_s. On the right picture in Fig. 10 the trajectories of these singular points start at values $x/a=\pm 3.4$ and continue to particle surface (which they reach at $\varepsilon''=0.58$). Within the first region the phase portrait contains two saddles (see phase portraits on the top part of Fig. 10). This phase portrait is similar to those shown in Fig. 8. Separatrices within the phase portrait clearly indicate the regions with input and output windows and the regions with plasmon emission–reabsorption fluxes).

(II) The second region with $0.2892<\varepsilon''<0.322$ is characterized by three roots with different ρ values. An upper
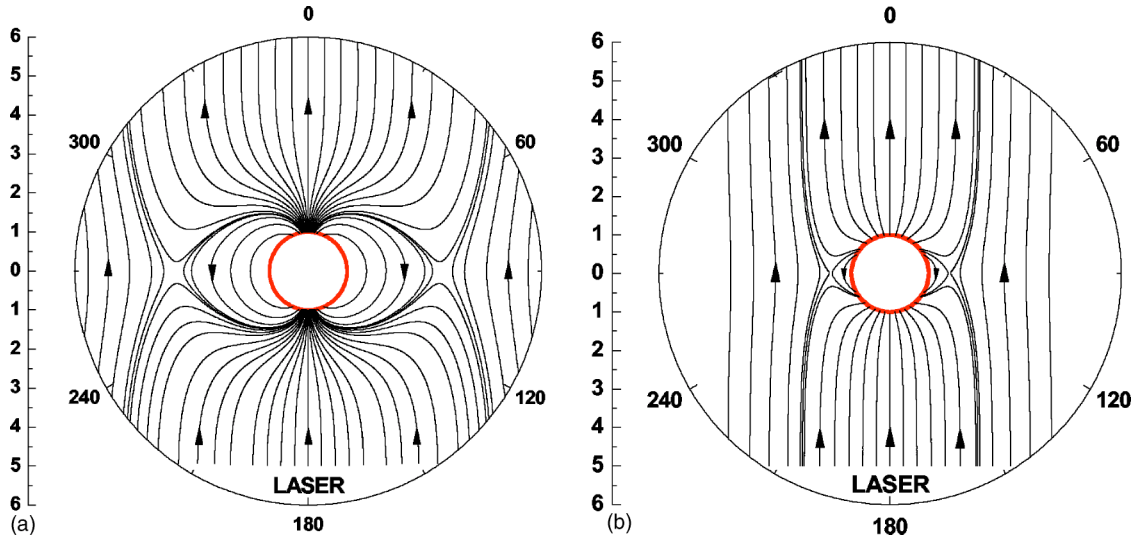
FIG. 8. Field lines in the *xz*-plane for a particle with a size parameter $q=0.3$ and permittivity $\varepsilon''=0$. (a) $\varepsilon'=-2$ (plasmon resonance); (b) $\varepsilon'=-1$ (off-plasmon resonance).

(degenerate) root continues trajectories of saddles within the first region and two additional roots move along the *z*-axis ($x=0$); see the right picture in Fig. 10. These points arise above the surface at $z/a=1.37$ and then move in different *z*-directions. The "intermediate" root which corresponds to an unstable node (saddle-node in 3-D space, the energy comes to this point from directions perpendicular to the picture) moves up. The root with the smallest ρ value is of the saddle-type; it moves down along the *z*-axis and reaches the particle surface at $\varepsilon''=0.322$. One can see a typical phase portrait at $\varepsilon''=0.3$ on the upper part of Fig. 10. The existence of the saddle point singularities in wave fields is well known within the theory of the wave front dislocations.[34,38] The only difference is that these singularities were previously discussed for the distribution of electric field while we consider the distribution of the energy flux.

(III) The third region with $0.322<\varepsilon''<0.54$ is also characterized by three roots with different ρ values. But these roots are qualitatively different from the second region. At $\varepsilon''=0.322$ one saddle point disappears (enters into the particle) while the node point is converted into the saddle and

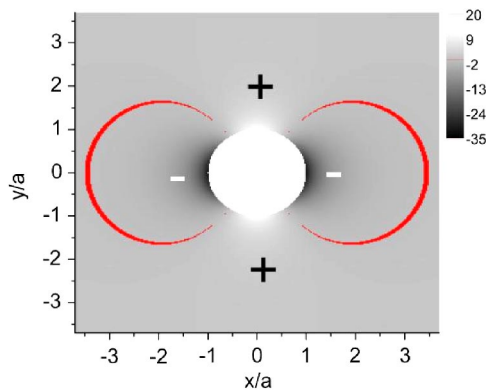

FIG. 9. (Color online) Contour plot of the S_Z component of the energy flux in an *xy*-plane at $z=0$. Negative energy flux (marked by the minus signs) is confined within two "tubes."

focus. The saddle point continues the branch of the roots which moves along the z-axes, while the branch with focus-type singular points is degenerated, it corresponds to two unstable foci (saddle-focus in 3-D space, the energy comes to this point from the directions perpendicular to the picture). On the right picture Fig. 10 the trajectories of these singular points correspond to two arcs above the particle, they continue till the particle surface (which they reach at $\varepsilon''=0.54$). The typical phase portrait for this region is presented in Fig. 10 for $\varepsilon''=0.37$. The behavior of fluxes in the vicinities of foci is similar to optical vortices, which were analyzed in many papers; see, e.g., Refs. 34, 39, and 40. But once again these singularities were previously discussed for the distribution of an electric field while we consider the distribution of the Poynting vector field. With an increase of an ε'' parameter the foci move to the surface (which they reach at $\varepsilon''=0.54$). The phase portrait at $\varepsilon''=0.48$ illustrates this motion.

(IV) The fourth region with $0.54<\varepsilon''<0.58$ is characterized by three saddle type points. The phase portrait for $\varepsilon''=0.55$ is shown at the bottom of Fig. 10. When the foci from region III enter the particle one can see on the top of the particle an emission–reabsorption process for plasmon.

(V) At $\varepsilon''>0.58$ two side's saddles from region IV disappear and the phase portrait has a single saddle point above the particle. Thus, for big dissipation we return to the Bohren's picture of flux, similar to those in Fig. 3.

One can see that an energy flux for a small particle has a number of bifurcations in the vicinity of plasmon resonance $\varepsilon'=-2$ with variation of dissipation parameter ε''. All of these bifurcations in the vector fields are quite general, similar bifurcations were found at wave front dislocations in the distribution of electric vector field (e.g. saddle,[38] focus,[34,39,40] node[41]). It is easy to verify that the Poynting vector fulfills the conservation law

$$\operatorname{div} \mathbf{S} = 0; \qquad (14)$$

this follows from the Maxwell equations. Thus vector field $\mathbf{S}_1 = \operatorname{curl} \mathbf{A}(r,\theta,\varphi)$ fulfills Eq. (14) with arbitrary vector $\mathbf{A}$
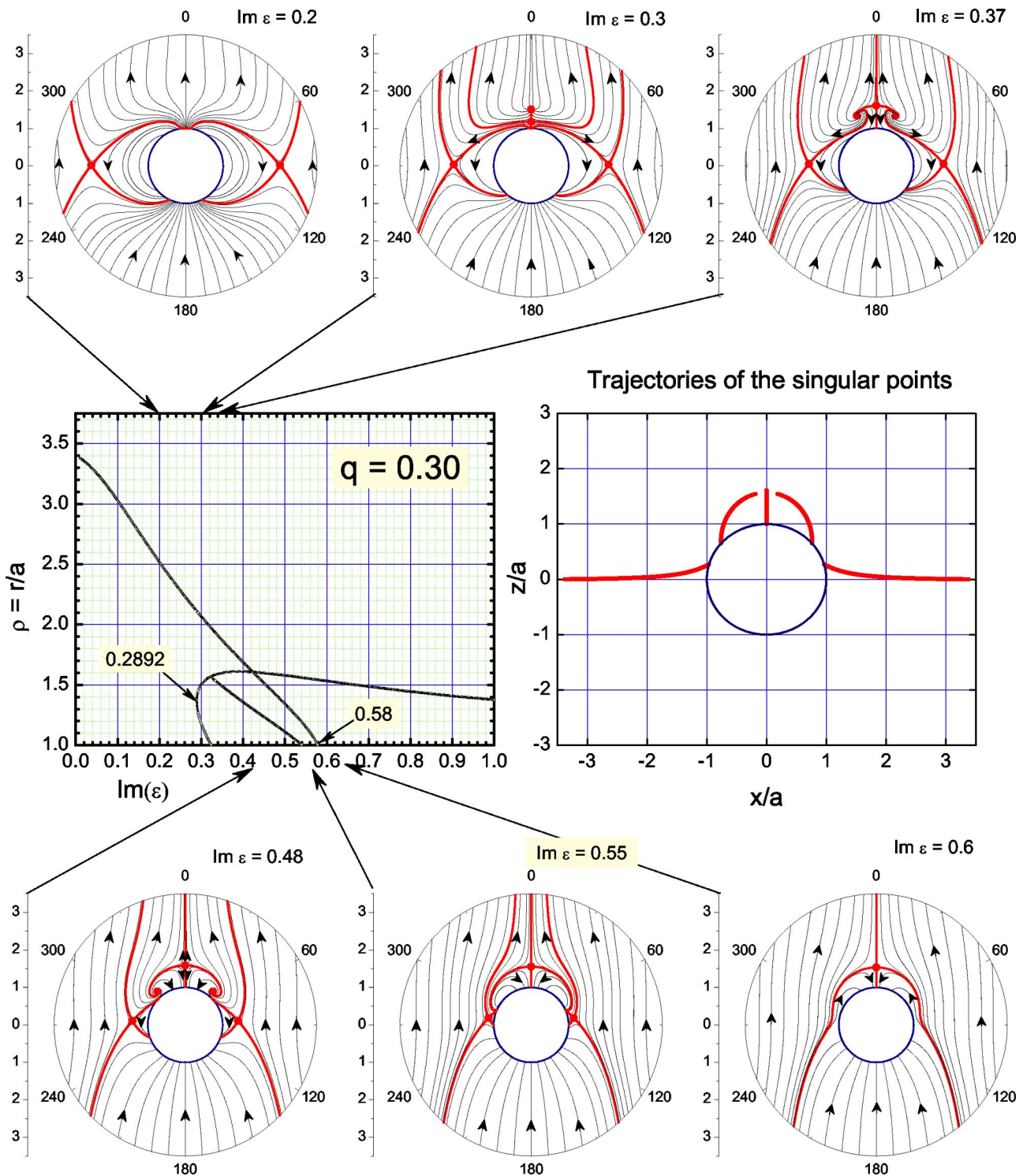
FIG. 10. (Color online) Field lines in the xz-plane for a particle with plasmon resonance $\varepsilon' = -2$ and size parameter $q = 0.3$. The central part of the picture presents stationary points and their trajectories versus ε''.

$=\mathbf{A}(r, \theta, \varphi)$. Another part is scalar field $u(r, \theta, \varphi)$, which should fulfill the Laplace equation: $\Delta u = 0$. Then vector $\mathbf{S}_2 = \mathrm{grad}\, u(r, \theta, \varphi)$ also fulfills Eq. (14). The construction of suitable vectors through electric and magnetic fields is quite complicated. For the case of cylindrical symmetry this problem was discussed in Ref. 42.

In conclusion, we have to add that the scattering of light by a small particle with plasmon resonance is attractive for applications in nanopatterning. For example, the nondissipative case is attractive for the generation of big electric and magnetic fields under the particle with plasmon resonance. For $q = 0.3$ and $\varepsilon'' = 0$ maximal value of the z-component of

the Poynting vector under the particle can reach $S_Z \approx 13$, while enhancements of corresponding electric and magnetic fields are $\mathbf{E}^2 \approx 200$ and $\mathbf{H}^2 \approx 15$.

IV. CONCLUSION

To describe the energy flux around the small particle near plasmon resonance the usual dipole approximation could be insufficient, because it produces an unstable energy flux. Such a situation arises for the case with small dissipation, when $\varepsilon = -2 + i\varepsilon''$ and $\varepsilon'' \ll 1$. Depending on the relation between the size parameter $q \ll 1$ and ε'', one should take into account more terms within the Mie series. Within the region of parameters that we used in calculations the stable phase portrait for the energy flux was reached when the number of terms were given by $\ell_{max} = q + 4.3 \, q^{1/3} + 1$. The nondissipative case with $\varepsilon'' = 0$ is characterized by input and output windows for the energy flux on the surface of the particle. With higher dissipation one can see a complex pattern of the energy flux in the vicinity of the particle. With big dissipation the energy flux enters the particle from any direction, i.e. one returns to the picture, typical for the dipole approximation. The case

with nondissipative damping would be attractive for many applications. It permits us to generate sufficiently high electric and magnetic fields in nanoscale around the particle in the near-field region.

APPENDIX:

Here we present the terms proportional to q^5 in electric and magnetic fields. These contributions arise from the first and second terms within the Mie series: $E^{(s)} = E^1(q^3) + E^1(q^5) + E^2(q^5)$. Terms $E^1(q^3)$ are given by Eq. (7) and terms $E^{1,2}(q^5)$ are given by

$$E_r^1(q^5) = \frac{6}{5}\frac{\varepsilon_p - 1}{(\varepsilon_p + 2)^2}q^5 \, e^{ikr}\frac{1 - ikr}{(kr)^3}(\varepsilon_p - 2)\sin\theta\cos\varphi,$$

$$E_r^2(q^5) = \frac{i}{2}\frac{\varepsilon_p - 1}{2\varepsilon_p + 3}q^5 e^{ikr}\frac{3 - 3ikr - (kr)^2}{(kr)^4}\sin 2\theta\cos\varphi,$$

$$E_\theta^1(q^5) = \frac{1}{30}\frac{\varepsilon_p - 1}{(\varepsilon_p + 2)^2}q^5 e^{ikr}\frac{[ikr + (kr)^2]\,(\varepsilon_p + 2)^2 + 18[-1 + ikr + (kr)^2](\varepsilon_p - 2)\cos\theta}{(kr)^3}\cos\varphi,$$

$$E_\theta^2(q^5) = \frac{1}{6}\frac{\varepsilon_p - 1}{2\varepsilon_p + 3}q^5 e^{ikr}\frac{-6i - 6kr + 3i(kr)^2 + (kr)^3}{(kr)^4}\cos 2\theta\cos\varphi,$$

$$E_\varphi^1(q^5) = -\frac{1}{30}\frac{\varepsilon_p - 1}{(\varepsilon_p + 2)^2}q^5 \, e^{ikr}\frac{18[-1 + ikr + (kr)^2](\varepsilon_p - 2) + [ikr + (kr)^2]\,(\varepsilon_p + 2)^2\cos\theta}{(kr)^3}\sin\varphi,$$

$$E_\varphi^2(q^5) = -\frac{1}{6}\frac{\varepsilon_p - 1}{2\varepsilon_p + 3}q^5 \, e^{ikr}\frac{-6i - 6kr + 3i(kr)^2 + (kr)^3}{(kr)^4}\cos\theta\sin\varphi. \tag{A1}$$

Similar terms in magnetic field $H^{1,2}(q^5)$ are given by

$$H_r^1(q^5) = \frac{\varepsilon_p - 1}{15}q^5 \, e^{ikr}\frac{1 - ikr}{(kr)^3}\sin\theta\sin\varphi, \quad H_r^2(q^5) = 0,$$

$$H_\theta^1(q^5) = \frac{1}{30}\frac{\varepsilon_p - 1}{(\varepsilon_p + 2)^2}q^5 e^{ikr}\frac{18[ikr + (kr)^2](\varepsilon_p - 2) + [-1 + ikr + (kr)^2](\varepsilon_p + 2)^2\cos\theta}{(kr)^3}\sin\varphi,$$

$$H_\theta^2(q^5) = \frac{1}{6}\frac{\varepsilon_p - 1}{2\varepsilon_p + 3}q^5 \, e^{ikr}\frac{-3 + 3ikr + (kr)^2}{(kr)^3}\cos\theta\sin\varphi,$$

$$H_\varphi^1(q^5) = \frac{1}{30}\frac{\varepsilon_p - 1}{(\varepsilon_p + 2)^2}q^5 e^{ikr}\frac{[-1 + ikr + (kr)^2](\varepsilon_p + 2)^2 + 18[ikr + (kr)^2](\varepsilon_p - 2)\cos\theta}{(kr)^3}\cos\varphi,$$

$$H_\varphi^2(q^5) = \frac{1}{6}\frac{\varepsilon_p - 1}{2\varepsilon_p + 3}q^5\, e^{ikr}\frac{-3 + 3ikr + (kr)^2}{(kr)^3}\cos 2\theta \cos \varphi. \tag{A2}$$

Within the xz-plane (i.e., $\varphi=0$) differential equation (9) is presented in the form of Eq. (10), where the numerator $F^{(num)}=\Sigma_{k=0}^4 u_k\rho^k$ and denominator $F^{(den)}=\Sigma_{k=0}^4 w_k\rho^k$ are given by the fourth order of polynomials (with respect to ρ). We present coefficients for the case where $\varepsilon_p=-2+i\varepsilon''$. Strokes in ε'' are omitted within the long formulas (A3) and (A4). The coefficients for the numerator are given by

$$u_0 = u_0^1 q, \quad u_1 = u_1^0 + u_1^2 q^2, \quad u_2 = u_2^1 q + u_2^3 q^3,$$

$$u_3 = u_3^2 q^2 + u_3^4 q^4, \quad u_4 = 1. \tag{A3}$$

Here terms u_i^k are the coefficients at different orders of q^k. They are equal to

$$u_0^1 = p\, \cos(2\theta)\sec\, \theta[5\varepsilon\, \cos\, \xi - (3 + 2\varepsilon^2)\sin\, \xi],$$

$$u_1^0 = -\cos\, \xi - \frac{3}{\varepsilon}\sin\, \xi,$$

$$u_1^2 = -\frac{p}{30\varepsilon^2}(3u_{c1}\cos\, \xi + \varepsilon u_{s1}\sin\, \xi),$$

$$u_{c1} = \frac{-72 + 5\varepsilon^2}{p} + 5\varepsilon^2(3 + 2\varepsilon^2)(2 + \cos\, \theta)\cos(2\theta)\sec\, \theta,$$

$$u_{s1} = \frac{126 + \varepsilon^2}{p} + 75\varepsilon^2(2 + \cos\, \theta)\cos(2\theta)\sec\, \theta,$$

$$u_2^1 = 2\cos^2\frac{\theta}{2}\left(-\frac{3}{\varepsilon}\cos\, \xi + \sin\, \xi\right),$$

$$u_2^3 = \frac{p}{15\varepsilon^2}\cos^2\frac{\theta}{2}\sec\, \theta(\varepsilon\, u_{c2}\cos\, \xi + 3\, u_{s2}\sin\, \xi),$$

$$u_{c2} = -\frac{\varepsilon^2 + 126\cos\, \theta}{p} - 75\varepsilon^2\cos(2\theta),$$

$$u_{s2} = \frac{-\varepsilon^2 + 6(-12 + \varepsilon^2)\cos\, \theta}{p} + 5\varepsilon^2(3 + 2\varepsilon^2)\cos(2\theta),$$

$$u_3^2 = 2\, \cos^2\frac{\theta}{2}\left(\cos\, \xi + \frac{3}{\varepsilon}\sin\, \xi\right),$$

$$u_3^4 = \frac{p}{15\varepsilon^2}\cos^2\frac{\theta}{2}\sec\, \theta(u_{c3}\cos\, \xi + \varepsilon\, u_{s3}\sin\, \xi),$$

$$u_{c3} = \frac{3}{p}[-\varepsilon^2 + 6(-12 + \varepsilon^2)\cos\, \theta] + 5\varepsilon^2(3 + 2\varepsilon^2)\cos(2\theta),$$

$$u_{s3} = \frac{\varepsilon^2 + 126\cos\, \theta}{p} + 25\varepsilon^2\cos(2\theta),$$

where $p=(1+4\varepsilon^2)^{-1}$.

Coefficients w_k for denominator have a similar form:

$$w_0 = w_0^1 q, \quad w_1 = w_1^0 + w_1^2 q^2, \quad w_2 = w_2^1 q + w_2^3 q^3,$$

$$w_3 = w_3^2 q^2 + w_3^4 q^4, \quad w_4 = 1. \tag{A4}$$

where w_i^k functions are presented by

$$w_0^1 = 3\, p\, \cos\, \theta[-5\varepsilon\, \cos\, \xi + (3 + 2\varepsilon^2)\sin\, \xi],$$

$$w_1^0 = 2\, \cos\, \xi + \frac{6}{\varepsilon}\sin\, \xi,$$

$$w_1^2 = -\frac{p}{30\varepsilon^2}(3\, w_{c1}\, \cos\, \xi + \varepsilon\, w_{s1}\, \sin\, \xi),$$

$$w_{c1} = 144 + 563\varepsilon^2 - 52\varepsilon^4 + 5\varepsilon^2(3 + 2\varepsilon^2)[-6\cos\, \theta + \cos(2\theta)],$$

$$w_{s1} = \frac{-252 + \varepsilon^2}{p} + 75\varepsilon^2[-6\cos\, \theta + \cos(2\theta)],$$

$$w_2^1 = (-2 + \cos\, \theta)\left(-\frac{3}{\varepsilon}\cos\, \xi + \sin\, \xi\right),$$

$$w_2^3 = \frac{p}{30\varepsilon^2}(-\varepsilon\, w_{c2}\cos\, \xi + 3\, w_{s2}\sin\, \xi),$$

$$w_{c2} = -\frac{-252 + \varepsilon^2}{p} + 6(21 + 59\varepsilon^2)\cos\, \theta + 75\, \varepsilon^2\cos(2\theta),$$

$$w_{s2} = 144 + 563\, \varepsilon^2 - 52\, \varepsilon^4 + 4(-18 - 78\varepsilon^2 + \varepsilon^4)\cos\, \theta + 5\varepsilon^2(3 + 2\varepsilon^2)\cos(2\theta),$$

$$w_3^2 = \cos\, \theta\left(\cos\, \xi + \frac{3}{\varepsilon}\sin\, \xi\right),$$

$$w_3^4 = \frac{p}{30\varepsilon^2}(w_{c3}\cos\, \xi + \varepsilon\, w_{s3}\sin\, \xi),$$

$$w_{c3} = \frac{3}{p}[-\varepsilon^2 + 6(-12 + \varepsilon^2)\cos\, \theta] + 5\varepsilon^2(3 + 2\varepsilon^2)\cos(2\theta),$$

$$w_{s3} = \frac{\varepsilon^2 + 126 \cos \theta}{p} + 25\varepsilon^2\cos(2\theta).$$

Substituting (A3) and (A4) into the formulas for numerator $F^{(\text{num})}$ and denominator $F^{(\text{den})}$ one can derive differential equation for the field lines.

---

*Corresponding author: Electronic address: Boris_LUKIYANCHUK@dsi.a-star.edu.sg

[1] M. Born and E. Wolf, *Principles of Optics*, 7th ed. (Cambridge University Press, Cambride, 1999).

[2] P. W. Barber and S. C. Hill, *Light Scattering by Particles: Computational Methods* (World Scientific, Singapore, 1990).

[3] C. F. Bohren and D. R. Huffman, *Absorption and Scattering of Light by Small Particles* (Wiley, New York, 1983).

[4] J. W. Belcher and S. Olbert, Am. J. Phys. **71**, 220 (2003).

[5] A. Keiling, J. R. Wygant, C. A. Catell, F. S. Mozer, and C. T. Russell, Science **299**, 383 (2003).

[6] I. V. Dzedolik, Tech. Phys. Lett. **29**, 194 (2003).

[7] W. Żakowich, Phys. Rev. E **64**, 066610 (2001).

[8] S. M. Huang, M. H. Hong, B. S. Luk'yanchuk, Y. W. Zheng, W. D. Song, Y. F. Lu, and T. C. Chong, J. Appl. Phys. **92**, 2495 (2002).

[9] S. Papernov and A. W. Schmid, J. Appl. Phys. **92**, 5720 (2002).

[10] S. M. Huang, M. H. Hong, B. S. Luk'yanchuk, and T. C. Chong, Appl. Phys. A: Mater. Sci. Process. **77**, 293 (2003).

[11] J. R. Krenn, A. Dereux, J. C. Weeber *et al.*, Phys. Rev. Lett. **82**, 2590 (1999).

[12] J. R. Arias-Gonzales and M. Nieto-Vesperinas, Opt. Lett. **25**, 782 (2000).

[13] M. Quinten, Appl. Phys. B: Lasers Opt. **73**, 245 (2001).

[14] *Laser Cleaning*, edited by B. Luk'yanchuk (World Scientific, New Jersey, 2002).

[15] B. S. Luk'yanchuk, N. Arnold, S. M. Huang, Z. B. Wang, and M. H. Hong, Appl. Phys. A: Mater. Sci. Process. **77**, 209 (2003).

[16] P.-M. Adam, S. Benrezzak, J. L. Bijeon, and P. Royer, J. Appl. Phys. **88**, 6919 (2000).

[17] Y.-S. Choi, H. J. Moon, K. Y. An, S. B. Lee, J. H. Lee, and J. S. Chang, J. Korean Phys. Soc. **39**, 928 (2001).

[18] J. C. Knight, N. Dubreuil, J. Hare *et al.*, Opt. Lett. **20**, 1515 (1995).

[19] C. Liu, T. Weigel, and G. Schweiger, Opt. Commun. **185**, 249 (2000).

[20] M. H. Fields, J. Popp, and R. K. Chang, in *Progress in Optics*, edited by E. Wolf (Elsevier, Amsterdam, 2000), Vol. 41.

[21] S. Nie and S. R. Emmony, Science **275**, 1102 (1997).

[22] J. P. Kottmann and O. J. F. Martin, Opt. Express **8**, 655 (2001).

[23] K. Li, M. I. Stockman, and D. J. Bergman, Phys. Rev. Lett. **91**, 227402 (2003).

[24] C. F. Bohren, Am. J. Phys. **51**, 323 (1983).

[25] M. I. Tribelsky, Sov. Phys. JETP **59**, 534 (1984).

[26] P. G. Kik, S. A. Maier, and H. A. Atwater, Mater. Res. Soc. Symp. Proc. **705**, Y3.6 (2002).

[27] S. M. Huang, B. S. Luk'yanchuk, M. H. Hong, and T. C. Chong, Appl. Phys. Lett. **82**, 4809 (2003).

[28] Yu. A. Kravtsov and Yu. I. Orlov, *Geometrical Optics of Inhomogeneous Media* (Springer-Verlag, Berlin, 1990).

[29] M. Ohtsu and H. Hori, *Near-field Nano-Optics* (Kluwer Academic, New York, 1999).

[30] V. M. Agranovich and V. L. Ginzburg, *Crystal Optics with Spatial Dispersion, and Excitons* (Springer-Verlag, Berlin, 1984).

[31] J. A. Stratton, *Electromagnetic Theory* (McGraw-Hill, New York, 1941).

[32] L. D. Landau and E. M. Lifshitz, *Electrodynamics of Continuous Media* (Pergamon, New York, 1994).

[33] S. Wolfram, MATHEMATICA, 4th edition (Wolfram Media/Cambridge University Press, Cambridge, 1999).

[34] M. Vasnetsov and K. Staliunas, *Optical Vortices* (Nova Science Publ., Commack, 1999).

[35] V. I. Arnold, *Catastrophe Theory*, 3rd ed. (Springer-Verlag, Berlin, 1992).

[36] T. Poston and I. Stuart, *Catastrophe Theory and its Applications* (Pitman, London, 1978).

[37] M. I. Rabinovich and D. I. Trubetskov, *Oscillations and Waves in Linear and Nonlinear Systems* (Kluwer Academic, Dordrecht, 1989).

[38] I. Freund, Opt. Commun. **163**, 230 (1999).

[39] M. V. Berry, J. Opt. A: Pure Appl. Opt. **6**, 259 (2004).

[40] A. V. Voluar and T. A. Fadeeva, Opt. Spectrosc. **85**, 272 (1998).

[41] V. P. Aksenov, I. V. Izmailov, B. N. Poizner, and O. V. Tikhomirova, Opt. Spectrosc. **92**, 409 (2002).

[42] R. Horak, Z. Bouchal, and J. Bajer, Opt. Commun. **133**, 315 (1997).